Supporting Information

A Mechanically Robust Polyurethane Elastomer with Excellent Crack Tolerance, recyclability and Weathering Resistance via Microphase Dynamic Ordering

Rongchi Zhang[a], Xuanbao Xiang[a], Donghai Sheng[a], Lin Zhang[a,*], Wanmeng Ren[a], Guoxin Xie[a], Shutao Wei[b], Huilian Dai[b]

a State Key Laboratory of Tribology in Advanced Equipment, Department of Mechanical Engineering, Tsinghua University, Beijing 100084, China
b 361°(CHINA)Co., Ltd, Xiamen Fujian 361000, China
** Corresponding author. E-mail: Lin Zhang (zhanglin2020@mail.tsinghua.edu.cn)*

1. Characterizations

Gel Permeation Chromatography (GPC): The molecular weight and its distribution of elastomers were measured through GPC (Waters 1515 GPC system, Waters Corporation, US). The samples were dissolved in DMF with 0.06 M LiBr at 50 ℃ with a flow rate of 1.0 mL·min^{-1} and an injection volume of 50 μL. H Nuclear Magnetic Resonance Spectra (^{1}H NMR): The ^{1}H NMR spectra were collected on a Brucker AV-HD-600X (600 MHz) spectrometer using DMSO-d6 as solvent. Fourier Transform Infrared Spectrometer (FTIR): The functional groups of PU samples were characterized through FTIR (X70, NETZSCH, Germany) with scanning of 32 times and scanning wave number range of 4000 cm^{-1} to 400 cm^{-1}. X-ray Diffraction (XRD): XRD tests were carried out on a D/max-2550(Rigaku, Japan) with Cu Kα radiation. The scanning range was 10 °- 80 ° with a scanning speed of 10 °·min^{-1}. Small Angle X-ray Scattering (SAXS): 2D-SAXS patterns were obtained on a Xeuss SAXS/WAXS system (Xenocs, France) equipped with a semiconductor detector (Pilatus R 300K, DECTRIS, Switzerland) attached to a multilayer focused Cu Kα X-ray source (GeniX3D Cu ULD, Xenocs, France). The wavelength of X-ray was 0.154 nm. The distance from the sample to the detector was 1165 mm and the exposure time was 60 min. The long period (L) was calculated by Bragg's law:

$$L = \frac{2\pi}{q} \tag{1}$$

where q is the value of the intensity curves (I(q) ~ q). The scattering vector $q = 4\pi(sin\theta)/\lambda$, where λ is the wavelength of X-ray and θ is half of the scattering angle (2θ). Atomic Force Microscopy (AFM): The microstructure of elastomers was determined by AFM (Probe name: AC160, Dimension, Bruker, Germany) using tapping mode with a scan area of 1 × 1 μm^2. Transparency Test: Transparency tests were conducted with a UV-vis spectrophotometer (PE Lambda950). The scanning wavelength was 800 nm - 400 nm and air was selected as reference. Differential Scanning Calorimeter (DSC): DSC data of samples were recorded on a Q5000IR DSC (TA Instruments, America) instrument. During the first cycle, the heat range was from -90 ℃ to 150 ℃ with a heating rate of 20 ℃·min^{-1}, and samples were then cooled to -

90 ℃ with a cooling rate of 20 ℃·min^{-1}. All data were collected in the second process to eliminate the thermal history, with samples being heated from -90 ℃ to 150 ℃ with a heating rate of 10 ℃·min^{-1} under nitrogen atmosphere. Thermal Gravimetric Analysis (TGA): Samples of PU elastomers were heated from 25 ℃ to 600 ℃ at a rate of 20 ℃·min^{-1} on a Q5000IR TGA device (TA Instruments, America). All tests were under nitrogen atmosphere. Dynamic Mechanical Analysis (DMA): Dynamic mechanical analyses were performed on the DMA Q800 (Waters, America) under film tension mode with an initial prestress of 0.01 N, a dynamic strain of 0.1 % and a fixed frequency of 1 Hz. The scanning temperature was -90 ℃ to 100 ℃ with a heating rate of 3 ℃·min^{-1}. Stress relaxation test was also conducted on the DMA instrument, during which the samples were maintained under stretching of 100 % strain for 30-minutes relaxation.

Tensile tests: Tensile tests were carried out on an electronic testing machine (AGX-V, Shimadzu, Japan) with a 20 kN load cell. Sample elastomers were cast into dumbbell-shape with an effective area of 20 mm × 5 mm × 3 mm. All tests were performed at a stretching rate of 50 mm·min^{-1}. True stress (σ_t) and true strain (ϵ_t) were calculated according to the engineering stress-strain curve with following equations respectively:

$$\sigma_t = \sigma * \frac{L}{L_0} = \sigma(1+\epsilon) \tag{2}$$

$$\epsilon_t = \int_{L_0}^{L} \frac{dL}{L} = ln(1+\epsilon) \tag{3}$$

where σ is the engineering stress, ϵ is the engineering strain, L is the current length of samples under deformation and L_0 is the original length of samples. Toughness of samples was obtained by integrating engineering stress (σ) over engineering strain (ϵ), represented by the area under stress-strain curves at a stretching rate of 50 mm·min^{-1}. Following equation was used:

$$Toughness = \int_{\epsilon=0}^{\epsilon_{max}} \sigma d\epsilon \tag{4}$$

where σ is the engineering stress, ϵ is the engineering strain and ϵ_{max} is the elongation at break of samples.

Cycle tensile tests: The cycle tensile tests were conducted at a constant deforming rate of 50 mm·min^{-1} during the stretching and releasing period. In each cycle, once the tensile strain set in advance was reached, the moving direction of the sample clamp was reversed and the strain was decreased to zero at the same rate. Immediately after zero stress had been reached, the clamp reversed its moving direction again and the sample was then stretched till the next target strain. The cycle tests were circularly performed until the last cycle was completed. For continuous cyclic stretching test, the samples were stretched to 100 % strain for 50 cycles based on above procedures.

Fracture energy measurement: Fracture energy was obtained from the tensile stretching experiments employing the samples which were notched 1 mm long on a single edge (samples in length of 20 mm, width of 5 mm and thickness of 1.25 mm) and all tests were conducted at a stretching rate of 50 mm·min^{-1}. The fracture energy (G_c) was calculated by the following equation:[1]

$$G_c = \frac{6wc}{\sqrt{\lambda_c}} \tag{5}$$

where c is the length of the notch (1 mm here), λ_c is the elongation at break of the notched sample and w is the integral of the stress-strain curve of the unnotched sample before the strain of $\lambda_c - 1$. In addition, the effect of notch sharpness to fracture energy was also explored. Specifically, tests were conducted on samples with varied triangle-shaped notches, which possessed the same notch length (c = 1 mm) and different notch widths (base of the triangle = 1 mm, 2 mm and 3 mm) and were located in the middle of one edge of the tested samples.

Trouser tear test: Tear resistance of elastomers was measured by trouser tear tests at room temperature on an electronic universal testing machine AGX-V (Shimadzu, Japan), which was equipped with a 20 kN load cell. Samples were cropped into 40 mm × 20 mm rectangular films with a thickness of 1.25 mm and a 20 mm long tear cut along

the median. Figure 5c presented the diagram of the samples prepared for trouser tear tests. The stretching rate was 50 mm·min^{-1} and the tear energy was calculated by following equation:

$$Tear\ energy = \frac{\int_0^L FdL}{t \cdot L_{bulk}} \tag{6}$$

where $\int_0^L FdL$ represented the integrated area under the curve of load F versus displacement L, t represented the thickness of the sample and L_{bulk} represented the length of the tear.

Healing efficiency: The healing efficiency of the elastomer were evaluated on a dumbbell-shaped sample (20 mm × 5 mm × 3 mm). For heat healing, the sample was cut down the middle and the incisions were immediately contacted, after which it was heated to heal under 100 ℃ for different durations. For solvent healing, the cut surfaces were coated with 0.6 uL trace solvent (DMSO), contacted and healed under room temperature for different time. The tensile tests were performed on the healed samples at a stretching rate of 50 mm·min^{-1}. The healing efficiency was determined with tensile strength (η_σ) and elongation at break (η_ϵ) and was calculated based on following equations:

$$\eta_\sigma = \frac{\sigma_h}{\sigma_0} \times 100\% \tag{7}$$

$$\eta_\epsilon = \frac{\epsilon_h}{\epsilon_0} \times 100\% \tag{8}$$

where σ_h and ϵ_h referred to the tensile strength and elongation at break of the healed sample, σ_0 and ϵ_0 for those parameters of the original sample.

Weathering resistance tests: Dumbbell-shaped samples (20 mm × 5 mm × 3 mm) were prepared and placed in different environments containing water, acid solvent (10% H_2SO_4), alkali solvent (10% NaOH), oil (PAO 40), 80℃ hot air and UV aging,

respectively. Samples were totally immersed in mentioned liquids, aged in oven or aged by UV lamp of 3.08 mW/cm^{-2} at 340 nm in a dark chamber (the sample-to-lamp distance was 2 cm). Tensile tests were conducted on aged samples. The degradation rates of strength (η_s) and elongation at break (η_e) were calculated as followed:

$$\eta_s = \frac{\sigma_d - \sigma_0}{\sigma_0} \times 100\% \tag{9}$$

$$\eta_e = \frac{\epsilon_d - \epsilon_0}{\epsilon_0} \times 100\% \tag{10}$$

where σ_d and ϵ_d referred to the tensile strength and elongation at break of the degraded sample, σ_0 and ϵ_0 for those parameters of the original sample. Besides, samples under water, NaOH, H_2SO_4 and PAO oil were weighed in different time durations to measure their mass variations.

2. Supporting figures

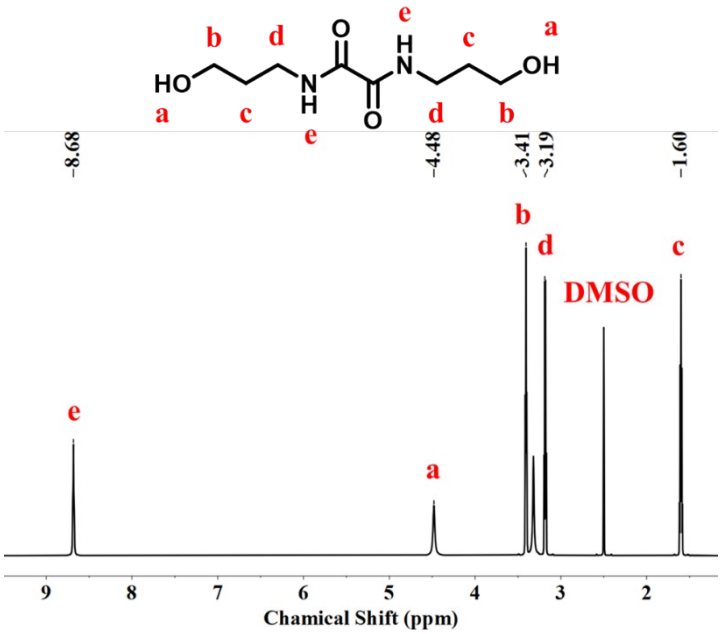

Figure S1. [1]HNMR spectrum of BPO dissolved in DMSO-d_6.

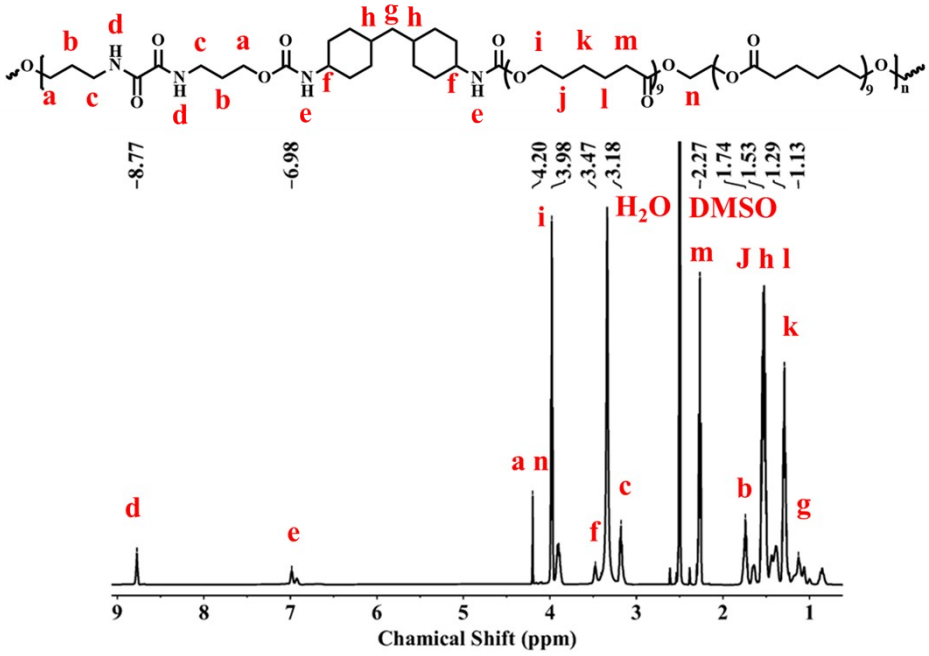

Figure S2. [1]HNMR spectrum of HMDI-PCL-BPO dissolved in DMSO-d_6.

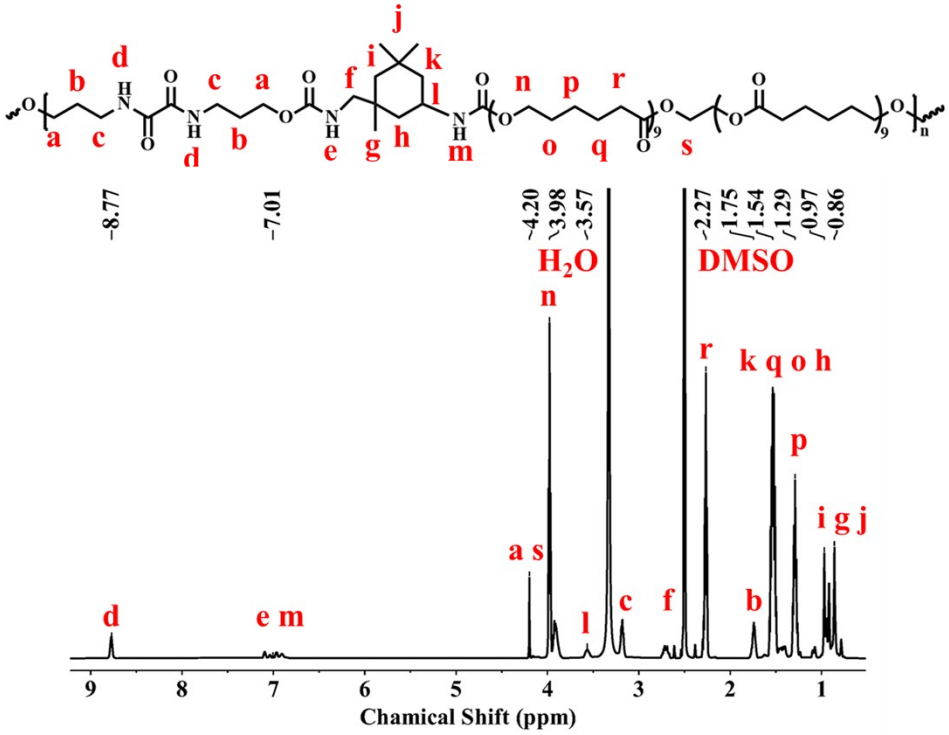

Figure S3. [1]HNMR spectrum of IPDI-PCL-BPO dissolved in DMSO-d_6.

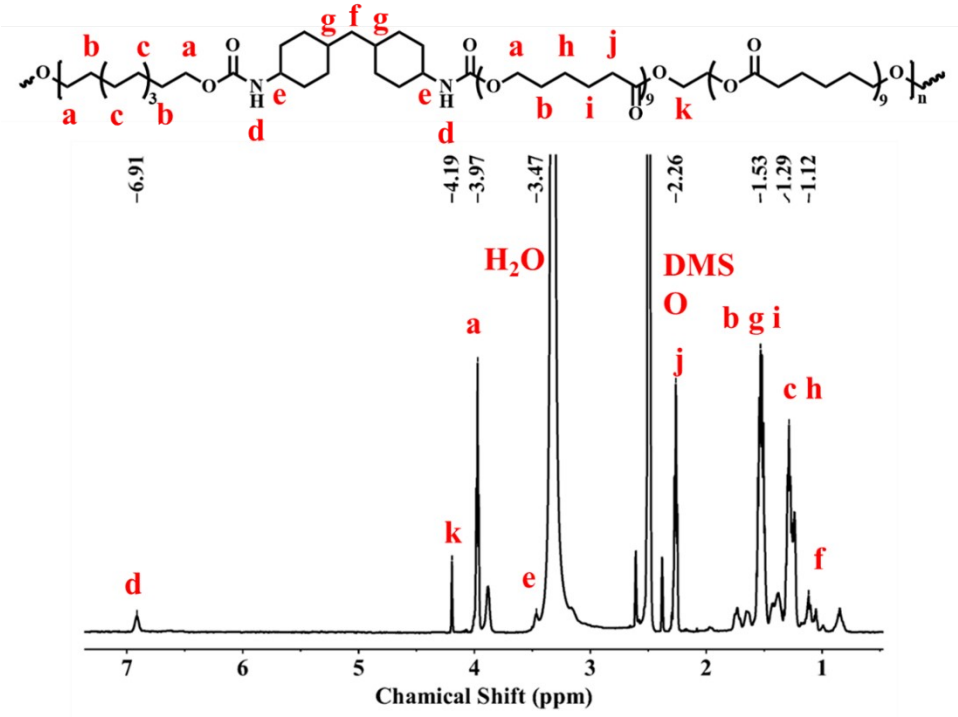

Figure S4. [1]HNMR spectrum of HMDI-PCL-DDO dissolved in DMSO-d_6.

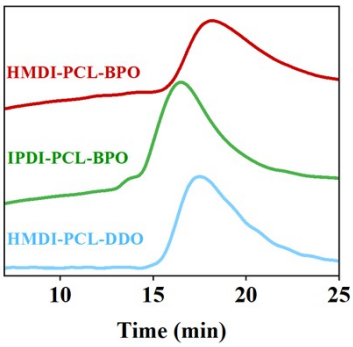

Figure S5. GPC traces of HMDI-PCL-BPO, IPDI-PCL-BPO and HMDI-PCL-DDO with DMF as the elution solvent.

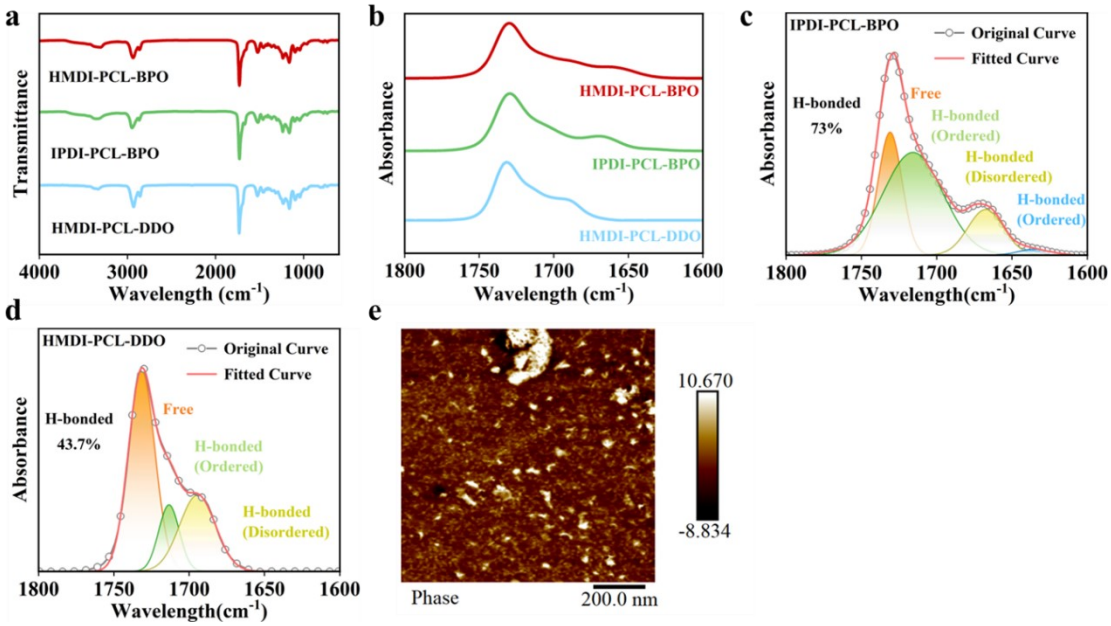

Figure S6. (a)(b) FTIR spectra of elastomers in wavenumber range of 4000 – 400 cm^{-1} (a) and of 1800 – 1600 cm^{-1} (b). **(c)(d)** Deconvoluted FTIR spectra of elastomers in the C=O vibration region. **(e)** AFM phase diagram of HMDI-PCL-DDO.

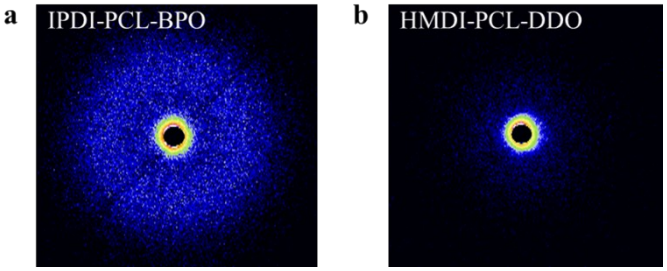

Figure S7. (a)(b) 2D SAXS profiles of IPDI-PCL-BPO (a) and HMDI-PCL-DDO (b).

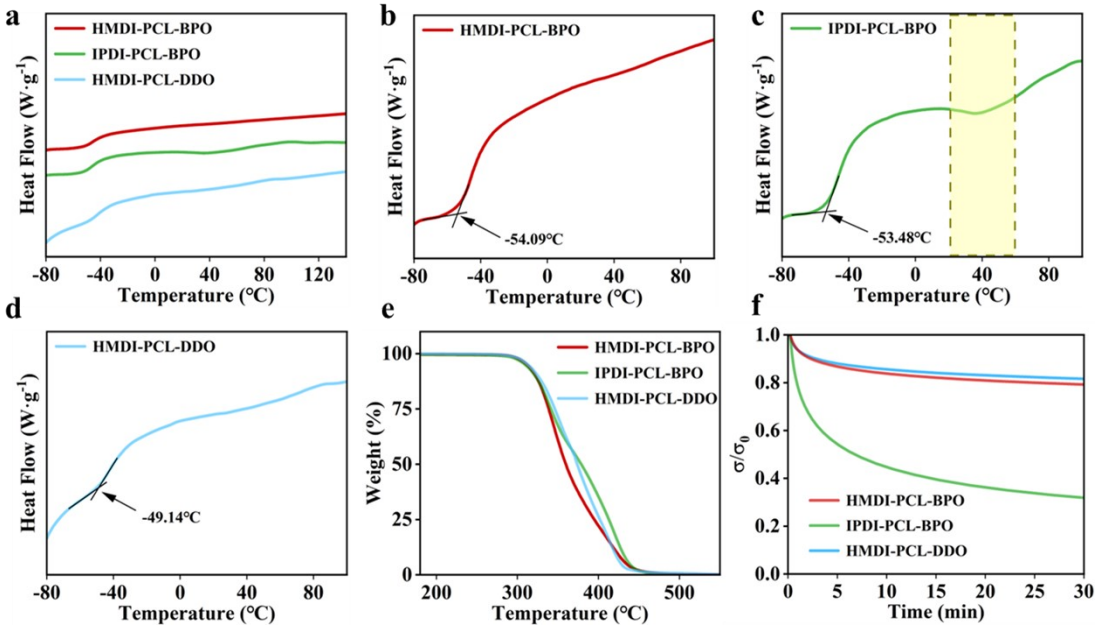

Figure S8. (a)-(d) DSC curves of elastomers (a), including HMDI-PCL-BPO (b), IPDI-PCL-BPO (c) and HMDI-PCL-DDO (d). **(e)** TGA curves of elastomers. **(f)** Normalized stress relaxation results of samples at ambient condition.

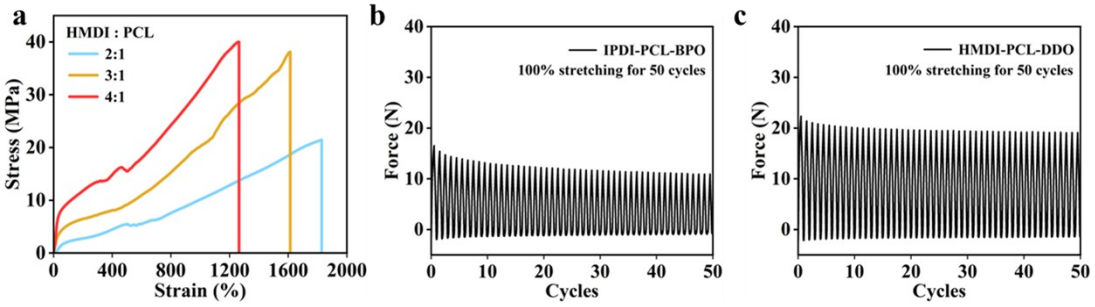

Figure S9. (a) Engineering stress-strain curve of HMDI-PCL-BPO samples with different R values. **(b)(c)** Cyclic stretching tests of IPDI-PCL-BPO (a) and HMDI-PCL-DDO (b) at 100% strain for 50 cycles.

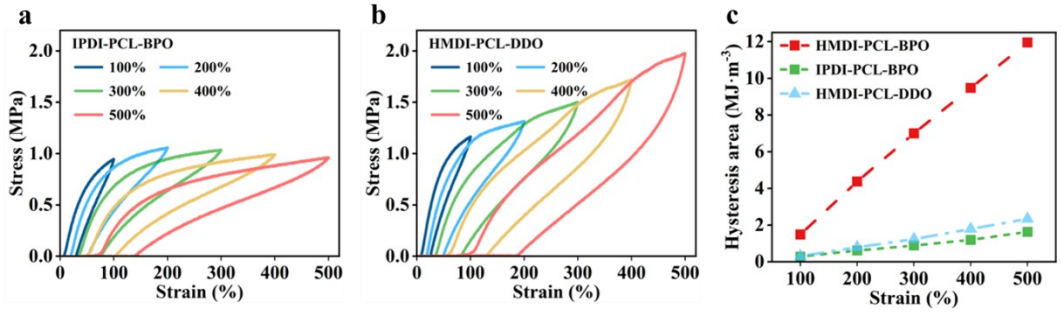

Figure S10. (a)(b) Loading-unloading curves of IPDI-PCL-BPO (a) and HMDI-PCL-DDO under different strains. **(c)** Hysteresis areas of each loading cycle of elastomers.

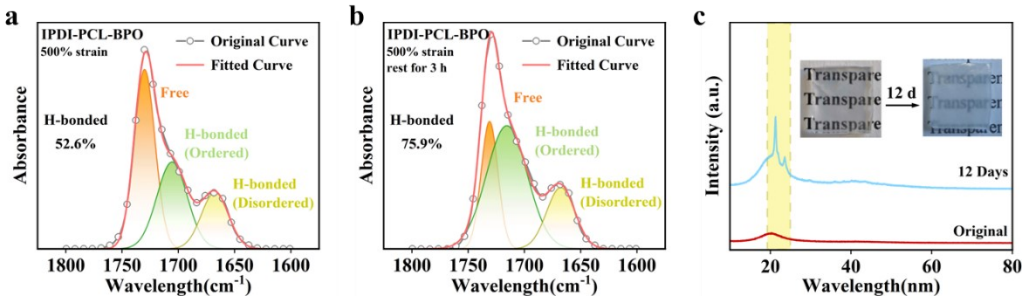

Figure S11. (a)(b) FTIR spectra in C=O vibration region of IPDI-PCL-BPO samples being stretched to 500% (a) and then resting for 3 h (b). **(c)** XRD spectra of IPDI-PCL-BPO being left to stand for 12 days.

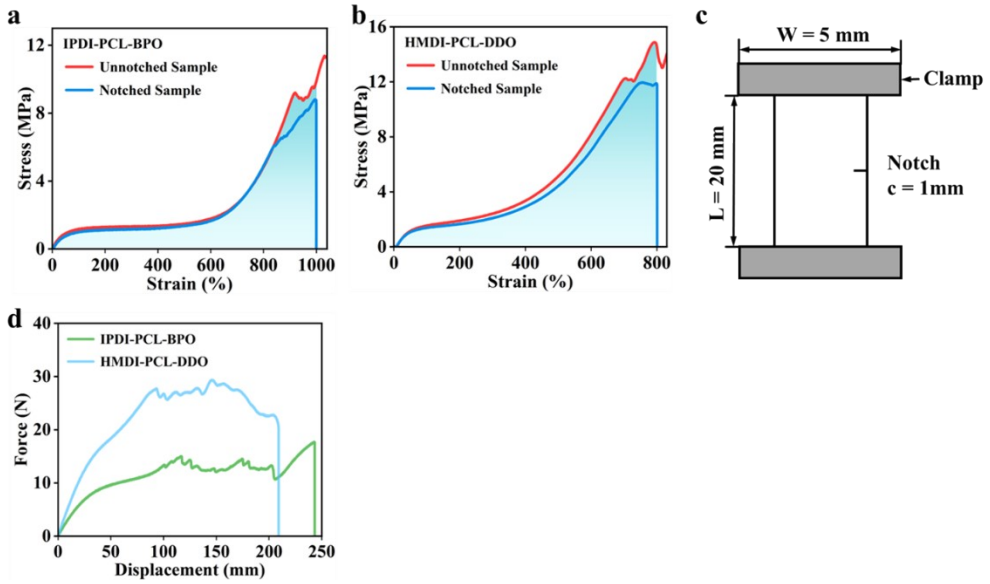

Figure S12. (a)(b) Tensile tests performed on notched samples of IPDI-PCL-BPO (a) and HMDI-PCL-DDO (b). **(c)** Diagram of notched samples. d) Trouser tearing tests of IPDI-PCL-BPO and HMDI-PCL-DDO.

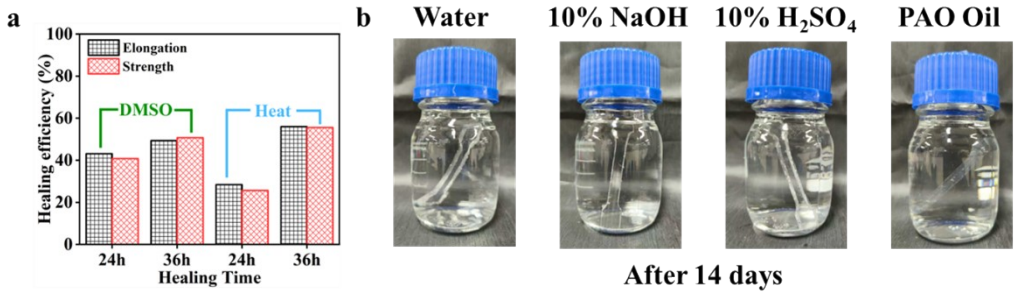

Figure S13. (a) Healing efficiency (calculated from the strength and elongation after healing) of HMDI-PCL-BPO versus healing time and healing methods. **(b)** Photographs of HMDI-PCL-BPO under different degradation conditions over 14 days.

3. Supporting Tables

Table S1. Stoichiometric ratio of samples.

Samples	HMDI [g]	IPDI [g]	PCL [g]	BPO [g]	DDO [g]	$n_{(-NCO)}/n_{(-OH)}$
HMDI-PCL-BPO	6.3	/	16	3.27	/	3:1
IPDI-PCL-BPO	/	5.4	16	3.27	/	3:1
HMDI-PCL-DDO	6.3	/	16	/	2.79	3:1
HMDI-PCL-BPO (2:1)	6.3	/	24	2.45	/	2:1
HMDI-PCL-BPO (4:1)	6.3	/	12	3.68	/	4:1

Table S2. Summary of molecular weight, polydispersity index, glass transition temperature (T_g) and temperature at 5% mass loss.

Samples	Mn [kDa]	Mw/Mn	Tg [℃]	Decompose 5% [℃]
HMDI-PCL-BPO	25.7	1.75	-54.1	311
IPDI-PCL-BPO	53.1	2.39	-53.5	309
HMDI-PCL-DDO	60.6	1.97	-49.1	313

Table S3. Summary of subpeaks deconvoluted from FTIR spectra in C=O vibration band and their ratios.

Assignment		Wavenumber (cm^{-1})			Area (%)		
		HMDI-PCL-BPO	IPDI-PCL-BPO	HMDI-PCL-DDO	HMDI-PCL-BPO	IPDI-PCL-BPO	HMDI-PCL-DDO
ν(C=O) urethane	Free	1731	1731	1731	26.8	27.0	56.3
	H-bonded (Disordered)	-	-	1713	-	-	14.6
	H-bonded (Ordered)	1716	1716	1694	52.4	56.4	29.1
ν(C=O) amide	H-bonded (Disordered)	1686	1667	-	5.4	14.9	-
	H-bonded (Ordered)	1660	1635	-	15.4	1.7	-
Total degree of H-bonded					**73.2**	**73.0**	**43.7**

Table S4. Summary of samples' mechanical properties.

Samples	Engineering stress [MPa]	Elongation at break [%]	Toughness [MJ·m^{-3}]	True stress [MPa]	True elongation [%]
HMDI-PCL-BPO	39.0±1.2	1558.8±38.4	275.8±5.2	646.4±19.3	2.8±0.02
IPDI-PCL-BPO	7.2±1.7	1288.1±91.7	38.2±11.0	99.9±29.5	2.6±0.06
HMDI-PCL-DDO	14.5±1.2	1584.8±77.6	87.5±11.2	243.9±28.1	2.8±0.05

Table S5. Comparisons of HMDI-PCL-BPO and other polyurethanes reported in literatures which were synthesized via solvent-free method.

Samples	Engineering stress [MPa]	Elongation at break [%]	Toughness [KJ·m^{-3}]
HMDI-PCL-BPO	39.0	1558.8	275.8
Ref 45	38.2	982.5	129.4
Ref 58	15.3	1200	100.8
Ref 59	16	383	/
Ref 60	45.5	621	/
Ref 61	45.12	864.9	/
Ref 62	17.4	497	/
Ref 63	150	16	/
Ref 64	10.9	977	/
Ref 65	32.2	780	/
Ref 66	35	140	/
Ref 67	3.23	70.4	/
Ref 68	17.5	158.7	41.61
Ref 69	20.1	1197.2	66.9
Ref 70	11.5	124.9	13.5

Table S6. Subpeak distributions, which were deconvoluted from FTIR spectra in C=O vibration band, of HMDI-PCL-BPO and IPDI-PCL-BPO at 500% strain and resting for 180 min.

Assignment		Wavenumber (cm^{-1})				Area (%)			
		500% Strain		Rest for 180 min		500% Strain		Rest for 180 min	
		HMDI-PCL-BPO	IPDI-PCL-BPO	HMDI-PCL-BPO	IPDI-PCL-BPO	HMDI-PCL-BPO	IPDI-PCL-BPO	HMDI-PCL-BPO	IPDI-PCL-BPO
ν(C=O) urethane	Free	1732	1730	1731	1731	21.5	47.4	26.9	24.1
	H-bonded (Ordered)	1716	1706	1716	1716	53.7	33.3	44.9	56.4
ν(C=O) amide	H-bonded (Disordered)	1688	1667	1686	1667	5.9	19.3	12.6	19.5
	H-bonded (Ordered)	1665	-	1660	-	18.9	-	15.6	-

Total degree of H-bonded	**78.5**	**52.6**	**73.1**	**75.9**

4. References

1 H. W. Greensmith, 1963, **7**, 993-1002, DOI: 10.1002/app.1963.070070316